Ninth International Conference on CFD in the Minerals and Process Industries
CSIRO, Melbourne, Australia
10-12 December 2012

CFD MODELLING OF A SUBSEA COOLER FOR CALCULATION OF EXTERNAL HEAT TRANSFER COEFFICIENT

Martin LEAHY[1*], Deepak JAGANNATHA[1], Christian CHAUVET[2] and James HOLBEACH[1]

[1] MSi Kenny, 432 Murray St Perth, Western Australia 6000, AUSTRALIA
[2] MSi Kenny, Caledonian House, 234 Union Street Aberdeen, AB10 1TN, SCOTLAND
*Corresponding author, E-mail address: martin.leahy@msikenny.com

ABSTRACT

A subsea heat exchanger was designed to meet the cooling demand of reducing the pipeline inlet temperature of production fluid. Computational Fluid Dynamics (CFD) was used to model the external heat transfer in a network of pipes representing the subsea cooler. For computational simplicity only the pipe wall and surrounding water domain were modelled, with internal temperature prediction being calculated separately in a one-dimensional model and iteratively incorporated into the CFD model. The system was set up under quiescent conditions, and a purely natural convection flow regime was allowed to develop. For the base case heat exchanger configuration considered, the overall heat transfer coefficient found was 753 $Wm^{-2}K^{-1}$. Sensitivity cases were considered to observe the effect of offsetting the pipes and lifting the subsea cooler higher off the seabed. Modest improvements were gained by such adjustments. The lifting case had the strongest effect with 5% increase in the external heat transfer coefficient (EHTC), whilst the offset case had a 1% increase in the EHTC.

NOMENCLATURE

C_p	specific heat
g	gravity vector
h	enthalpy
k	thermal conductivity
k	kinetic energy
p'	modified pressure
Pr	Prandtl number
T	temperature
v	velocity
β	thermal expansivity
ρ	density
μ	dynamic viscosity
ω	eddy frequency

Subscripts

T	turbulent
ref	reference
amb	ambient
$cond$	conductivity

INTRODUCTION

The subsea cooler is a heat exchanger (HXC) that relies on cool seawater to pass over the exposed pipes containing hot gas condensate stream. The cooling of the raw gas typically occurs via a combination of forced and natural convection of seawater, depending on the seawater current conditions. Internally water and oil condense along the length of the heat exchanger as the production fluids cool. This results in changes to the internal heat transfer characteristics and the hydraulics of the system. Although there are several designs commonly used in the industry, it is not straightforward to obtain the correct size of the HXC in order to achieve a certain cooling requirement. This is because the internal gas temperature drop, which depends heavily on obtaining an accurate external heat transfer coefficient (EHTC), is required. Other considerations are also important, such as minimizing the size and weight (for cost of building and commissioning) whilst also limiting internal hydraulic losses. (This is due to a trade off between smaller pipe for good heat exchange and larger pipe for reduced pressure drop.) Furthermore, there is scope for improving the design of the HXC, because the HXC requires structural support and dropped object / strike / trawl over protection, which may be optimized through careful configuration design. Therefore, there is scope for a study to predict more accurately the EHTC for a subsea cooler.

The heat transfer properties of vertical array of straight pipes in natural convection are relatively well understood [1-2], with the studies indicating the elevation, spacing and inclination play an important role, along with the Rayleigh and Grashof numbers. Recently, Gyles et.al. [3] conducted an experimental study on a specific cooler design using Large Eddy Simulation (LES) to study the heat transfer from one cylinder/pipe. Absence of information available for detailed heat transfer from a complex subsea HXC and the calculation of the internal gas temperature from the outlet are the motivations for the present study.

METHODOLOGY

There are several computational tools that may be used to carry out the design and optimization, including OLGA (a one-dimensional mechanistic and empirically based multiphase simulator) and fully three-dimensional multiphase computational fluid dynamics (CFD). We used a combination of these tools iteratively to arrive at a converged solution, as shown in Figure 1. In this work only initialisation step 1 and initialisation step 2 are discussed, with initialisation step 2 (CFD solution) being the main area of discussion. In future work, we will discuss the remaining iterative solution.

Copyright © 2012 CSIRO Australia

Although both natural and forced convection will occur in a real subsea environment, only natural convection was considered in this work since this is typically the sizing case for such equipment.

The modelled geometry included pipe walls and flow of seawater outside the pipe but no structural aspects that might hinder natural convection. This will be considered in later work.

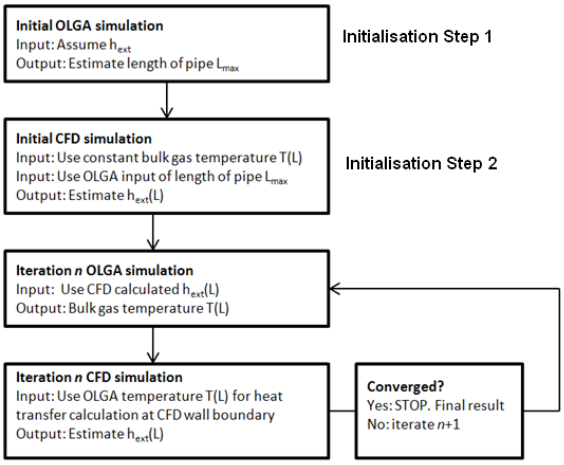

Figure 1 Flow diagram for iteration solution to obtain subsea cooler exit gas temperature

MODEL DESCRIPTION

Model Geometry

The schematic of the CFD model used in the present study is shown in Figure 2. Only the external surface of the cooler pipelines along with the sea water domain was modelled. A seawater bounding box was set up with a 2m buffer to each edge of the subsea cooler, except the base where the seabed was taken to be 0.4m from the cooler. This domain size was domain independent because opening pressure boundaries were used, which could handle recirculation zones across their faces.

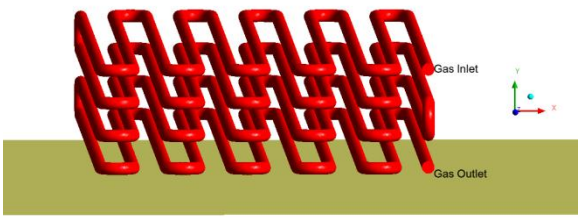

Figure 2: Schematic diagram of geometry, with pipes coloured red and seabed in sandy colour. Gas inlet and outlet were not used in the CFD calculation but are indicated for reference.

Meshing

ANSYS meshing software available within Workbench 14.0 was used to discretise the computational domain into finite volumes. Figure 3 and Figure 4 show the computational mesh used in the present study. An inflation layer (15 cells thick) was set up around each of the pipes to ensure the y+ was around 1 to accurately resolve the temperature and velocity field close to the pipe. The domain immediately surrounding and in between the pipes was filled with tetrahedral mesh elements, while the outer sea water domain was filled with hexahedral mesh elements. The mesh was checked to satisfy the quality criterion. The total number of elements was 25 million and number of nodes was 8 million. Mesh independence tests were carried out, with acceptable levels of mesh dependence.

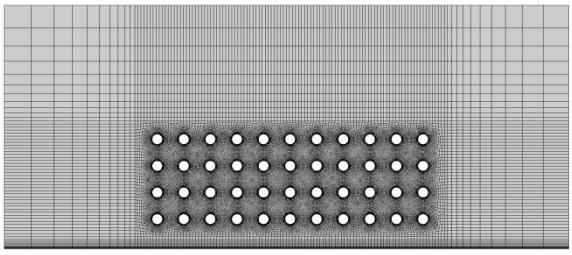

Figure 3: Slice at mid XY plane showing computational mesh.

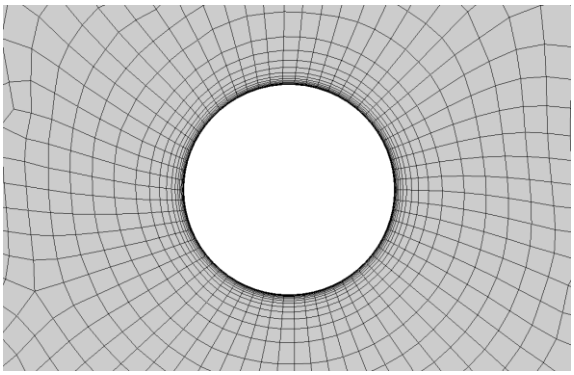

Figure 4 Close-up of mesh near the surface of pipe

Theory

The following section describes the modelling procedure and theory. The CFD model was set up within the ANSYS CFX v14 framework [4]. In the sea water domain the model was a single-phase model that solved the Navier-Stokes equations. A steady state solution was calculated, as this was a good first approximation to the flow that developed. A transient formulation could be used for finishing the steady state solution, due to transient features related to the flow around pipes and other unsteady features of the subsea cooler. In this work only the steady state results are presented, as this provides a reasonable time-averaged approximation to the flow. The equation of continuity is given by

$$\nabla \cdot (\rho \mathbf{v}) = 0 \tag{1}$$

and the momentum equation is given by

$$\nabla \cdot (\rho \mathbf{v}\mathbf{v}) = -\nabla p' + \nabla \cdot [(\mu + \mu_T)(\nabla.\mathbf{v} + \nabla.\mathbf{v}^T)] + \mathbf{B} \tag{2}$$

where ρ is the water density (assumed constant), $\mathbf{v}$ is the velocity, p' is the (modified) pressure (including the hydrostatic part $-\rho\mathbf{g}.\mathbf{x}$), $\mathbf{g}$ (m s^{-2}) is the gravity vector and $\mathbf{B}$ is the natural convection buoyancy force, described below. The laminar viscosity is denoted μ (kg m^{-1} s^{-1}), and μ_T (kg m^{-1} s^{-1}) is the turbulent viscosity, described in equation (5).

An additional body force term to account for the buoyancy forces due to heating of the water from the pipes is given by

Copyright © 2012 CSIRO Australia

$$\mathbf{B} = -\rho \mathbf{g} \beta (T - T_{ref}) \quad (3)$$

where T (K) is the temperature of the water, T_{ref} (K) is chosen to be the ambient temperature, T_{amb}, and β (K^{-1}) is the thermal expansivity coefficient for water. The buoyancy force term described in Equation (3) is that of the well known Boussinesq approximation. Normally the Boussinesq approximation should be limited to cases with reasonably small variations in the temperature. In this work there are predominately small variations in the temperature (of a few degrees), but close to the walls there is a large variation in temperature. In future work we will consider the use of a full buoyancy model, with fully temperature-dependent water density.

The steady state transport equation for the enthalpy is given by

$$\nabla \cdot (h\mathbf{v}) = \nabla \cdot [(k_{cond} + C_p \frac{\mu_T}{Pr_T}) \nabla (\frac{T}{\rho})] \quad (4)$$

where Pr_T (-) is the turbulence Prandtl number taken as 0.9, and k_{cond} (W m^{-1} K^{-1}) is the thermal conductivity of sea water, C_p (J kg^{-1} K^{-1}) is heat capacity of sea water.

The turbulent viscosity μ_T in equations (2) and (4) is determined by solving transport equations for the SST k-ω turbulence model. The SST k-ω model has good close-to-wall behaviour (good velocity profile prediction), and is thus used. SST k-ω requires integration to the wall to accurately predict heat transfer, thus deeming k-ε based turbulence models unsuitable. The turbulent viscosity can be written in terms of the transported variables - kinetic energy k (m^2 s^{-2}) and eddy frequency ω (s^{-1}) as

$$\mu_T = \rho \frac{k}{\omega} \quad (5)$$

Table 1 shows the constants used in the sea water domain based on 3.5% salinity [5]. The properties for the constants were evaluated at ambient seawater temperature T_{amb}.

Constants	Definition	Value	Units
ρ	Density	1024	kg m^{-3}
β	Thermal expansivity	0.0002	K^{-1}
k	Thermal conductivity	0.6014	W $m^{-1}K^{-1}$
C_p	Heat capacity	4190	J $kg^{-1}K^{-1}$
μ	Viscosity	0.00112	kg $m^{-1}s^{-1}$
T_{ref}	Reference temperature	18.5	°C
T_{amb}	Ambient temperature	18.5	°C

Table 1: Constant properties used for the seawater.

Boundary Conditions

To model the heat transfer from the pipes, a typical EHTC (9000 W/m^2K) for the internal high-speed gas flow and heat transfer through the steel pipe was used. This was based on a separate CFD calculation of the gas flow within the pipe, combined with simple analytical calculation of heat transfer through the pipe wall. An inner-wall temperature of 95°C was applied for the free-stream gas temperature. For the outer boundaries of the water domain, opening pressure boundary conditions were used to allow for recirculation zones that may develop; for these boundaries, the inflow temperature was set to T_{amb}=18.5°C. At all walls, no slip boundary conditions were applied. These boundary conditions provided stable convergence to residuals levels below 10^{-4}.

RESULTS

Cases

The base case (Case 1) was taken to be a standard design subsea cooler with inline pipes (i.e. pipes that sit directly above one another) at a nominal distance above the seabed (0.4m). Three sensitivity cases were considered: Case 2 - where the whole system of pipes was raised by 1m to 1.4m, Case 3 - where the pipes were offset evenly by one radius of curvature (and were 0.4m above the seabed), and Case 4 – a single isolated pipe, which was used for reference.

Case 1 - Base Case

The results for the base case are shown in Figure 5 - Figure 11. Natural convection drives flow into the bulk of the cooler and accelerated vertically, reaching maximum velocity above the cooler (Figure 5). Temperature contours are shown in Figure 6, indicating that there was lateral flow at the outer edges and vertical flow in the inner pipes, with the flow strongest at the top. A close up of the vectors plot (with temperature contours) is shown in Figure 7. The water temperature increased as it approached the pipe then decreased as it re-entered the bulk flow (at a lower temperature).

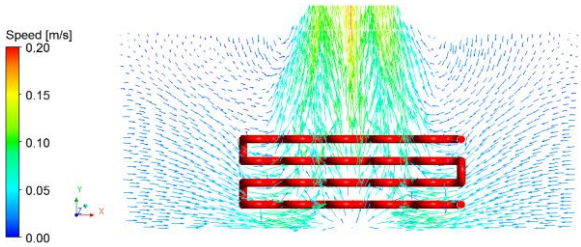

Figure 5 Velocity vectors of flow induced by natural convection at mid section slice.

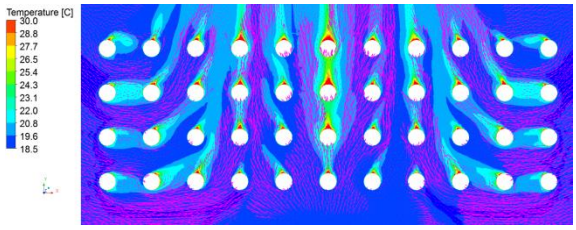

Figure 6 Velocity vectors (coloured pink) and temperature contours

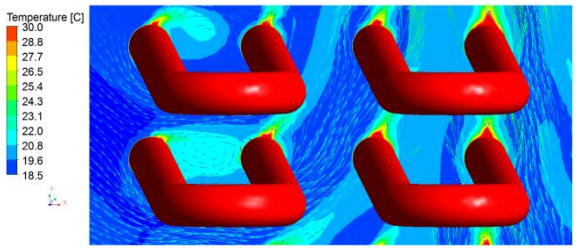

Figure 7 Close up of temperature contours and velocity vectors at mid section slice.

The EHTC on the wall of the top row and middle column of pipes is shown in Figure 8. Figure 8 shows the lowest

Copyright © 2012 CSIRO Australia

EHTC to be at the edges and toward the bottom. A line plot of the EHTC for each pipe, from one side of the cooler to the other, and for each pipe row is shown in Figure 9. There are three effects to note. Firstly, moving from one side to the other, the EHTC increases, locally peaks then levels out; the EHTC also displays symmetry from one side to the other. At the fourth pipe column, the peak that occurs can be explained by the higher velocity and having fresher (cooler) water, unlike the middle three pipes, which only have higher velocity. Secondly, the EHTC increases with increasing height. This can be explained by the fact that bottom has a lower velocity, compared to the higher pipe rows. This is despite the lower pipes having cooler water approaching the lower pipes. Thirdly, the bottom two rows show an increase in the EHTC at the outer pipes (C1 and C11). This can be explained by the cooler (ambient) water approaching the pipe, in addition to the higher velocities experienced (see Figure 6).

The wall temperature is shown in Figure 10 and Figure 11 from above and below respectively, indicating that the wall was hotter on the top of the pipes (due to reduced EHTC) and cooler on the underside and flanks of the pipe (where there was increased EHTC). Also, the trend for temperature versus pipe location from the edges had an inverse relationship to that of the EHTC (i.e. temperature is highest at the outer edges and decreases with height).

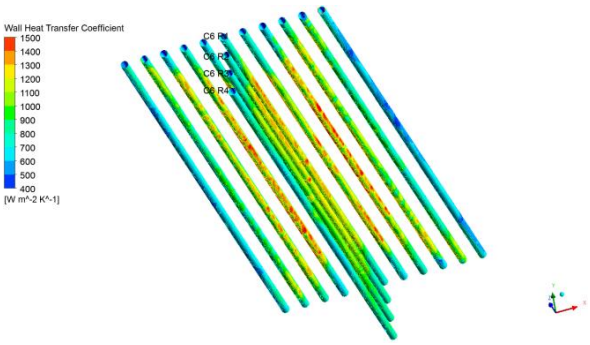

Figure 8 EHTC on the wall for selected pipes (top row and sixth column of pipes), viewed from below. Reference columns and rows are annotated with the column and row, using, for example, C6R1 as column 6, row 1

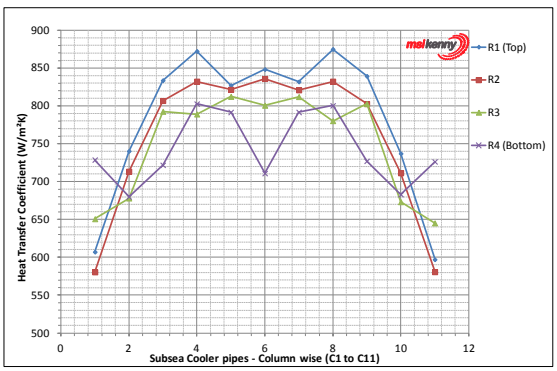

Figure 9 Line plot of EHTC for pipe column 1 to 11 (C1 to C11), for the four pipe rows (R1 to R4).

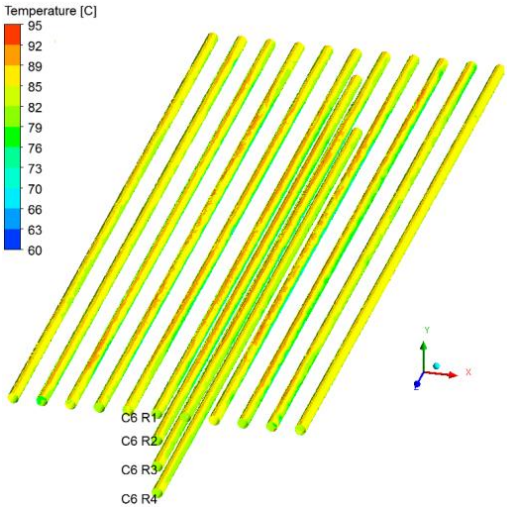

Figure 10 Wall temperature for the top row and middle column, viewed from above looking down. Reference columns and rows are annotated.

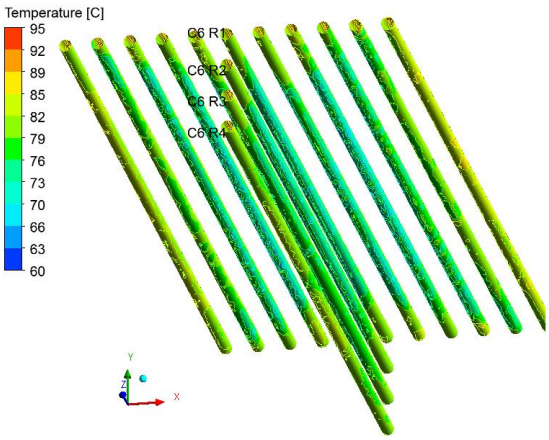

Figure 11 Wall temperature for the top row and middle column, viewed from below. Reference columns and rows are annotated.

Case 2 – 1.4m Lift

A sensitivity case where the system of pipes is lifted higher was considered: the pipes are lifted by 1m to 1.4m. Case 2 results are shown in Figure 12 and Figure 13 (vectors and temperature respectively). As expected, the lifted case showed more of a vertical flow pattern over more of the pipes, due to the lifted system, and a stronger flow speed. Consequently, the lifted cooler case allowed for a lower temperature over a significant portion of the pipes. The lower temperatures occured within the pipe network, especially at the fringes toward the top and bottom. The lower temperature was reflected in a high heat transfer coefficient, with a reasonable increase of 5% in the overall heat transfer coefficient as seen in Table 2

Copyright © 2012 CSIRO Australia

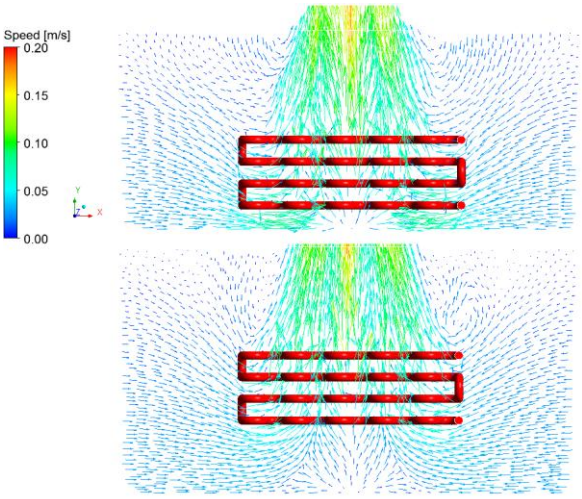

Figure 12 Velocity vectors for base case (top) and case 2 (bottom).

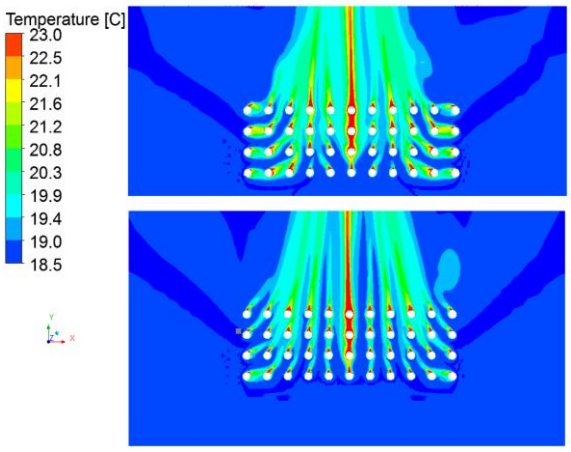

Figure 13 Temperature contours for base case (top) and case 2 (bottom).

Case 3 – Offset Pipes

Another sensitivity case was considered where the pipes are offset from one row to the next by one unit of radius of curvature (radius of curvature of the bends). This was to assess if the subsea cooler could be configured to optimize the EHTC. Figure 14 shows the temperature contours for the offset case (bottom) compared to the base case (top). The outer side pipes and bottom row of pipes received the same temperature profile on approach in both the base case and offset cases. However, the inner pipes received cooler water on approach to the pipes for the offset case. As a result the associated heat transfer was higher, and this was reflected in the modest increase of 1% in the overall heat transfer coefficient (as seen in Table 2).

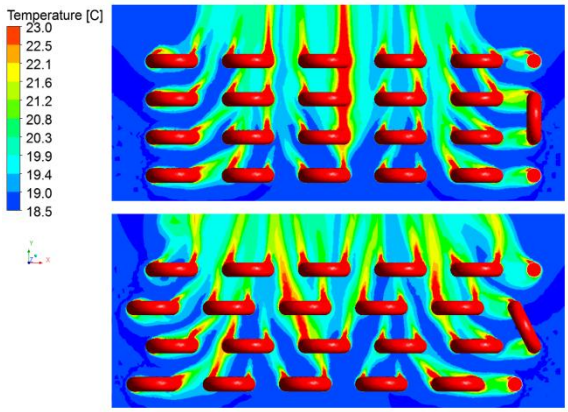

Figure 14 – Temperature contours for Case 3 (offset pipes case) (bottom) and case 1 (no offset) (top).

Case	Case Definition	Overall EHTC (W/m²/K)	% change EHTC
1	Base case	752.8	0
2	Base case – lift (1.4 m above seabed)	787.1	+5
3	Offset pipes	759.3	+1
4	Single isolated pipe	477.2	-36

Table 2: Summary of overall EHTC – base case and sensitivity cases.

Case 4 – Single isolated straight pipe

An additional case was also considered to establish the change in EHTC for the subsea cooler as a whole versus a single isolated pipe. The single pipe is isolated i.e. no other pipes are nearby. Table 2 shows the single pipe EHTC is 36% less than the base case for the full subsea cooler. This demonstrated the effect of grouping pipes together to increase the overall heat transfer coefficient. It also demonstrated the use of CFD to improve the estimate of the overall EHTC for input into OLGA, as opposed to calculating an EHTC for a single isolated pipe from empirical means.

DISCUSSION

The results presented showed the first CFD stage of the overall calculation routine shown in Figure 1. At this stage of the solution, it was assumed the internal wall temperature was constant along the length of the pipe. As a result the CFD results presented must be interpreted with a degree of caution. For example, the symmetry in the flow field observed is unlikely to be maintained completely when the temperature variance with pipe length (from OLGA) is used as input to CFD. This is due to the orientation of the pipe and the fact that the gas will be cooling as it travels along the pipe. Nevertheless, the results presented provide a reference case to assess the EHTC for the fully converged solution shown in Figure 1.

The sensitivity cases considered showed there to be a small effect of offsetting the pipes and lifting the subsea cooler higher off the seabed. The lifted case had the strongest effect with 5% increase in the EHTC, whilst the offset case had a 1% increase in the EHTC. These values are not significantly greater than other potential sources of

Copyright © 2012 CSIRO Australia

error, for example mesh dependence. Therefore further work is required to evaluate if these EHTC increases can be interpreted as real effects.

Future work will consider other geometry effects, such as strike protection shape optimization and spacings of pipes. We will also use a combination of CFD and OLGA to iterate between the external EHTC and the internal gas temperature so that the correct boundary conditions are applied to each domain. The properties of seawater as a function of temperature will also be included, as these may have an impact on the EHTC calculated. The Boussinesq approximation may also under predict the level of buoyancy at higher temperatures close to the pipe wall, due to the assumption of linearity of buoyancy force with respect to temperature variation. In future work we will also consider the use of a complete CFD solution, by solving for the flow in both the internal and external domains, and also modelling the heat transfer in the solid domain.

CONCLUSION

The external heat transfer coefficient for a realistic subsea cooler was calculated using CFD. Several important effects were elucidated, including the variation in EHTC as a function of position within the network. It was found that the EHTC increases with increasing row height, and that the inner pipes had the highest EHTC. Two other minor effects were also noted: (1) a local peak in the EHTC occurs, generally at the fourth pipe from the outside; and (2) in the bottom two rows there is a relative rise in the EHTC for the first and last columns (as compared to the top two rows). Sensitivity cases were considered, with modest improvements in the EHTC compared to the base case. These included lifting the cooler higher, with 5% higher EHTC, and offsetting the pipes, with 1% higher EHTC. A comparison was also made with a single isolated pipe, which showed 36% reduction in the EHTC; this shows there was a large effect from grouping the pipes reasonably close together to leverage the combined buoyancy of the system as a whole.

REFERENCES

ANSYS, (2012), CFX-14 Solver, ANSYS Inc., Canonsburg, USA, website address www.ansys.com/cfx

CHOUIKH, R., GUIZANI, A., MAALEJ, M., and BELGHITH, A. “Numerical study of the laminar natural convection flow around an array of two horizontal isothermal cylinders” *International Communication of Heat and Mass Transfer*, 26(3), 329-338 (1999).

GRAFSRØNNINGEN, S., JENSEN, A. and PETTERSSON-REIF, B.A. “PIV investigation of a buoyant plume above heated horizontal cylinder”, European Turbulence Conference, Warsaw, 2011

GRAFSRØNNINGEN, S., JENSEN A. and REIF A. *(2011)* "PIV investigation of buoyant plume from natural convection heat transfer above horizontal heated cylinder", *International Journal of Heat and Mass Transfer*, **54** (23-24), 4975-4987.

GYLES, B.R. “Natural Convection – Subsea Cooling; Theory, Simulations, Experiments and Design”, Proceedings of the ASME 2011 30th International Conference on Ocean, Offshore and Arctic Engineering, OMAE2011, June 19-24, 2011, Rotterdam.

MARSTERS, G.F, “Arrays of heated horizontal cylinders in natural convection”, *International Journal of Heat and Mass Transfer*, 15, 921-933 (1972).

SHARQAWYA, M.H., LIENHARD, J. AND ZUBAIRB S.M. “Thermophysical properties of seawater: a review of existing correlations and data” *Desalination and Water Treatment* **16**, 354–380, 2010.

Copyright © 2012 CSIRO Australia